Structural instabilities in disordered perovskites $Rb_{1-x}K_xCaF_3$ studied by synchrotron radiation powder diffraction. Proposition for a phase diagram

1998 J. Phys.: Condens. Matter 10 5485

(http://iopscience.iop.org/0953-8984/10/24/024)

J. Phys.: Condens. Matter **10** (1998) 5485–5502. Printed in the UK PII: S0953-8984(98)92053-7

Structural instabilities in disordered perovskites $Rb_{1-x}K_xCaF_3$ studied by synchrotron radiation powder diffraction. Proposition for a phase diagram

A Jouanneaux†§, Ph Daniel†‖ and G Bushnell-Wye‡¶

† Laboratoire de Physique de l'Etat Condensé, UPRES A CNRS No 6087, Université du Maine, Avenue Olivier Messiaen, 72085 Le Mans Cédex 9, France

‡ CLRC-Daresbury Laboratory, Daresbury, Warrington, Cheshire WA4 4AD, UK

Received 26 February 1998

Abstract. In the framework of general studies of structural phase transitions in disordered materials, the crystal structure of mixed perovskites $Rb_{1-x}K_xCaF_3$ has been investigated by high resolution powder diffraction using synchrotron radiation, for three selected impurity concentrations $x = 0.05, 0.20, 0.32$. The symmetries and space groups have been fully determined according to Glazer's formalism and the structures refined using the Rietveld method. Special attention was paid to pre-transitional effects and phase coexistence. Thanks to this thorough examination, a full phase diagram, transition temperature versus concentration, is suggested and interpreted from a model using the replica trick method and the mean field approximation. The validity of this model is discussed.

1. Introduction

In the last few years, the occurrence and nature of structural phase transitions (SPTs) in mixed crystal systems has become an intriguing topic, since the introduction of a structural disorder by an ionic substitution has until now not been well known in spite of numerous studies in this field (see for instance [1–3]). Moreover, the study of phase transitions in such mixed systems appears of great interest, especially in perovskites (AMX_3 compounds) which display a large variety of antiferrodistortive SPTs by rotation of the MX_6 octahedra around the main cubic axes.

In this framework, the mixed $Rb_{1-x}K_xCaF_3$ compounds can be considered as a model because the pure fluoroperovskites $RbCaF_3$ and $KCaF_3$, from which they are obtained, show evidence of competitive mechanisms for SPT and thus could demonstrate the existence of disorder in these mixed compounds.

Actually $RbCaF_3$ exhibits a first phase transition at 198 K [4] giving rise from the ideal cubic perovskite structure (see figure 1) to a tetragonal symmetry, corresponding to alternate rotations of CaF_6 octahedra around one of the major cubic axes (see for instance the review of Daniel *et al* [5] and references therein). This transition was shown to be

§ E-mail address: jouanneaux@univ-lemans.fr

‖ E-mail address: daniel@univ-lemans.fr

¶ E-mail address: g.bushnell-wye@dl.ac.uk

0953-8984/98/245485+18$19.50

structurally identical to the archetype perovskite $SrTiO_3$ [6] and related to the softening of the triply degenerate R'_{15} eigenmode located at the R(0.5, 0.5, 0.5) point of the first cubic Brillouin zone. The second transition occurring at $T_c = 31.5$ K [4, 5, 7, 8] gives rise to an orthorhombic symmetry without any group–subgroup relation with the tetragonal one and then this transition shows a first order character. In the case of $KCaF_3$, two SPTs were previously observed at high temperature [9–12]: the first at 560 K is due to the simultaneous condensation of eigenmodes located at the R(0.5, 0.5, 0.5) and M(0.5, 0, 0.5) points of the cubic Brillouin zone and the last occurring at 551 K is associated with an additional condensation of one component of one eigenmode at the R(0.5, 0.5, 0.5) point of the cubic reciprocal space. Finally it appears that in this kind of perovskite system, because of the existence of a quasi-flat R–M phonon branch, the mechanism of the phase transition can be associated either with the condensation of a mode located at the M point or with the R point of the reciprocal space. Consequently the rotations of the CaF_6 octahedra are either alternate around one main cubic axis or in the same sense, which corresponds to a natural competition between 'ferro' and 'antiferro' coupling of two adjacent octahedra planes perpendicular to a cubic rotation axis. The sequences of the SPTs occurring in the pure perovskites can be easily summarized using Glazer's classification [13]:

$$\mathrm{RbCaF_3}\left\{\begin{array}{c} a^0a^0a^0 \\ \text{cubic} \end{array}\right. \quad \begin{array}{c} T_{c1} = 198\ \mathrm{K} \\ \rightarrow \end{array} \quad \begin{array}{c} a^0a^0a^- \\ \text{tetragonal} \end{array} \quad \begin{array}{c} T_{c2} = 31.5\ \mathrm{K} \\ \rightarrow \end{array} \quad \begin{array}{c} a^-b^+a^- \text{ or } a^-a^+a^- \\ \text{orthorhombic} \end{array}$$

$$\mathrm{KCaF_3}\left\{\begin{array}{c} a^0a^0a^0 \\ \text{cubic} \end{array}\right. \quad \begin{array}{c} T_{c1} = 560\ \mathrm{K} \\ \rightarrow \end{array} \quad \begin{array}{c} a^0b^+c^- \\ \text{orthorhombic} \end{array} \quad \begin{array}{c} T_{c2} = 545\ \mathrm{K} \\ \rightarrow \end{array} \quad \begin{array}{c} a^-b^+c^- \\ \text{monoclinic} \end{array}$$

where the − superscript designates anti-phase tilts of CaF_6 octahedra, while the + superscript designates in-phase tilts, around pseudo-cubic axes. Furthermore the *a*, *b* and *c* pseudo-cubic axes are distinguished when tilt angles around these axes are different.

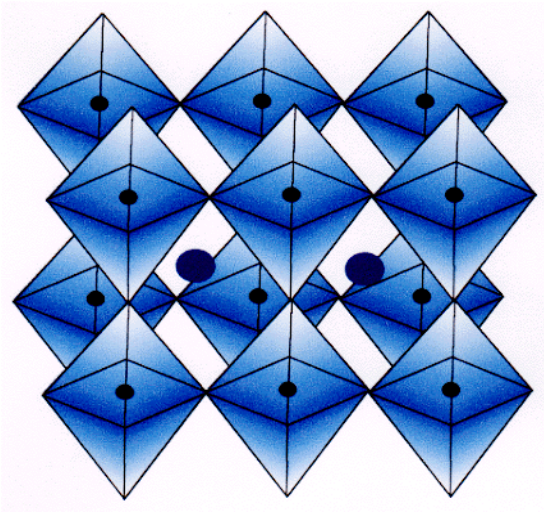

Figure 1. Ideal cubic aristotype perovskite ABX_3. Evidence of octahedron X_6 arrangement. The small solid circles are B bivalent cations, the large solid circles are A monovalent cations.

A first major study devoted to the mixed perovskites $Rb_{1-x}K_xCaF_3$ (with $0 < x < 1$) was performed by Foucher *et al* [14]; the transition temperatures versus concentrations

were determined by thermal analysis and the softening of the whole R–M phonon branch when approaching the transition was observed by inelastic neutron scattering. In a recent paper, the sequence of phase transitions in these compounds has been investigated using conventional powder diffraction [15]. However, because of very small lattice distortions, the symmetries in this system versus concentration cannot be determined unambiguously in most cases.

In this work, a full reinvestigation of the structural properties of the mixed perovskites $Rb_{1-x}K_xCaF_3$ has been performed for $x = 0.05$, 0.20 and 0.32 from high resolution x-ray powder diffraction using synchrotron radiation, in order to obtain definite answers about the symmetries in these compounds as well as to throw light on the pre-transitional effects. Also a new phase diagram is suggested in this article.

2. Experiment

2.1. Sample preparation

The powdered samples used for the experiments were obtained by crushing single crystals of $Rb_{1-x}K_xCaF_3$ compounds. These single crystals were grown by a modified Bridgmann–Stockbarger method [16] with an adapted protocol of temperature. For the three measured samples, the potassium concentration was previously checked by x-ray diffraction using Vegard's law.

2.2. Data collection

The high resolution x-ray powder diffraction patterns were recorded in Debye–Scherrer geometry on station 9.1 situated on the 5T wiggler of the 2 Gev SRS at Daresbury Laboratory. The sample was sieved at 10 μm and mounted in a Lindemann capillary of 0.2 mm diameter. Because of the small quantity of powder used in this technique, a good homogeneity in concentration can be expected for a given mixed compound.

A wavelength of 1.000 539(2) Å, slightly higher than that of the rubidium K absorption edge, was selected to avoid sample absorption effects as much as possible. The 2θ step size was 0.01°.

As these compounds show high diffracting power, rather short counting time per step was needed (of the order of one to two seconds per point). Therefore we did not use the sample spinning possibility available on the station. The capillary position was first manually adjusted to give a maximum of intensity for the most intense reflection in the pattern, and then kept fixed during all the measurements for a given concentration.

The samples were cooled using an Oxford Instruments He flow cryostat. The temperature was regulated with a precision of 0.1 K.

3. Data analysis

The powder diffraction patterns for each concentration at each measured temperature have been analysed by the Rietveld profile method [17]. All the refinements have been carried out using the program MPROF [18]. The scattering factors and anomalous dispersion terms were taken from [19] and [20] respectively. Rubidium and potassium atoms were statistically distributed over the same crystallographic site. Isotropic temperature factors

were refined and constrained to be equal for each atom type. Intensities were systematically corrected for sample absorption effects. As the powder compactness was not measured, the typical value of 60% was considered for each studied concentration. Therefore the effective (μr) value was 0.57, 0.55 and 0.54 for $x = 0.05$, 0.20 and 0.32 respectively.

Owing to the fixed capillary position, the appropriate correction was applied in MPROF to the peak positions arising from sample eccentricity in the cryostat. The values of the corresponding parameters were refined using the pattern of highest symmetry (that is the room temperature phase of cubic symmetry for $x \leqslant 0.32$) and then used as non-refined values for all other temperatures.

A slight anisotropic line broadening, probably due to the crushing sample preparation procedure, was detected on refining the pattern for $x = 0.20$. Therefore we applied a new method [21] able to handle qualitatively this effect. In this method, the U, V, W parameters in the Caglioti law [22], describing the peak width angular variation, are made hkl dependent as well as the pU, pV, pW parameters describing an angular variation of the peak shapes. Because of the super-Lorentzian character of the peak shapes, the Pearson VII function was found to give better results than the pseudo-Voigt one. Although a high number of profile refinable parameters is available in this method (36 in the general case), we have systematically limited this number to a few, mainly because the distortions encountered in these materials are weak and derived from the ideal pseudo-cubic symmetry. This anisotropic effect was not significant for other concentrations.

The space group (SG) determination was achieved by considering Glazer's [13] structural description for distorted perovskites by rotation of octahedra around their cubic axes. In these perovskites, the distortion type and the tilt system can be normally deduced from the splitting occurring on the (h00), (hh0), (hhh) or (hkk) main intense cubic reflections (indices are given in the pseudo-cubic supercell $2a \times 2b \times 2c$) as summarized in table 1, and then the structural phase transition sequence could be determined by monitoring characteristic diffraction peaks as a function of temperature. However in the case of very small splitting, the tilt system sometimes cannot be directly obtained from this method even with high resolution, as illustrated below for $x = 0.32$, and it is finally preferable to collect a pattern over a wider angular range involving not only the reflections mentioned above but also eventual superlattice reflections characteristic of + or − tilt systems. We have systematically adopted this data collection procedure which allows us to establish unambiguously the space group and to offer the other advantage that a full powder diffraction pattern is available for structural Rietveld refinements.

Table 1. Relation between the tilt systems and the number of reflections in a diffraction pattern. The indices and symmetries are related to the supercell $2a \times 2b \times 2c$.

Tilt system	h00	hh0	hhh	hkk	Symmetry
$a^0a^0a^0$	1	1	1	1	cubic
$a^0a^0c^-$	2	2	1	2	tetragonal
$a^0b^+b^-$	2	2	1	2	orthorhombic
$a^+b^+b^-$	2	2	1	2	orthorhombic
$a^-a^+a^-$	1	3	2	4	monoclinic
$a^-b^+a^-$	2	3	2	4	monoclinic
$a^-b^+c^-$	3	4	2	6	monoclinic

4. Results and discussion

4.1. $Rb_{0.95}K_{0.05}CaF_3$

As previously established, $Rb_{0.95}K_{0.05}CaF_3$ exhibits two SPTs [14, 15]: the first one at $T = 210$ K gives rise from the ideal cubic symmetry ($a^0a^0a^0$) to an orthogonal phase $I4/mcm$ ($a^0a^0c^-$) as in the pure $RbCaF_3$, and the second one occurs at $T = 74$ K. In order to investigate this lowest temperature phase, a diffraction pattern was recorded at $T = 50$ K in the range 12–65° 2θ, counting 2 s per step.

The tilt system (c^-) in the tetragonal phase produces, with respect to the cubic symmetry, some superlattice reflections whose indices in the double pseudo-cubic cell ($2a$, $2b$, $2c$) are of odd–odd–odd type with $h \neq k$, e.g. (311); (313) [13]. In the low temperature phase for $x = 0.05$, new reflections appear (figure 2), such as (321), (341), (501) (so-called M lines) and (320), (410), (412) (X lines). According to Glazer [13], the presence of M lines indicates a tilt $+$. Moreover the splitting of the (444) reflection into two components (figure 3) is consistent with a monoclinic distortion of the supercell $2a \times 2b \times 2c$. Then only the SGs $B2_1/m$ (No 11) and $Pnma$ (No 62) are allowed, the former being the more general one. The same result was obtained in pure $RbCaF_3$ [8] whose low temperature structure was finally solved from neutron powder diffraction data in SG $Pnma$ associated with a tilt system ($a^-a^+a^-$), after the refinement in $B2_1/m$ demonstrated a great tendency of equality of the cell constants and of the tilt angles. It is worth noting however that the $I4/mcm$ tetragonal to $Pnma$ orthorhombic transition does not correspond to a group–subgroup relation and so is normally associated with a first order character of the transition.

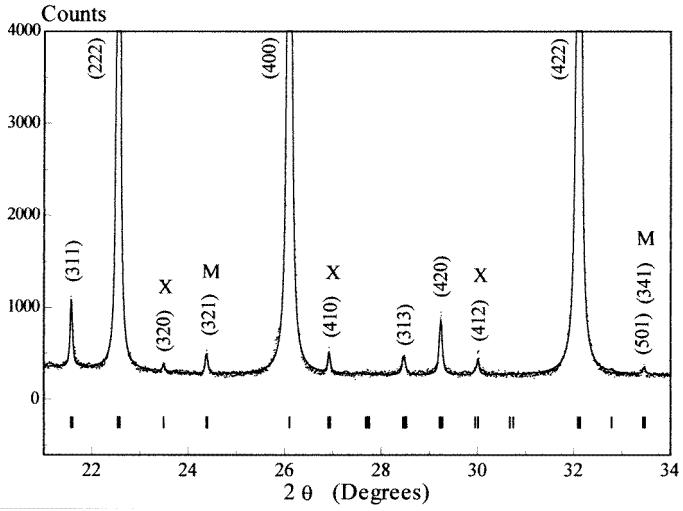

Figure 2. Part of observed and calculated profiles for $Rb_{0.95}K_{0.05}CaF_3$ collected at 50 K.

In $Rb_{0.95}K_{0.05}CaF_3$, the (400) reflection (figure 4) does not present any visible splitting; this indicates that the cell constants $2a$, $2b$, $2c$ have very close values. Therefore a first Rietveld refinement was performed with $2a = 2b = 2c$ together with constraints on the atomic displacements of fluorine and (Rb, K) atoms in agreement with the SG $Pnma$ consistent with an ($a^-a^+a^-$) tilt system. The restrictions are given in table 2 and the Rietveld results in table 3. As shown in figure 2, the fit is very satisfactory with well refined superlattice reflections. A Rietveld refinement was also performed in SG $B2_1/m$.

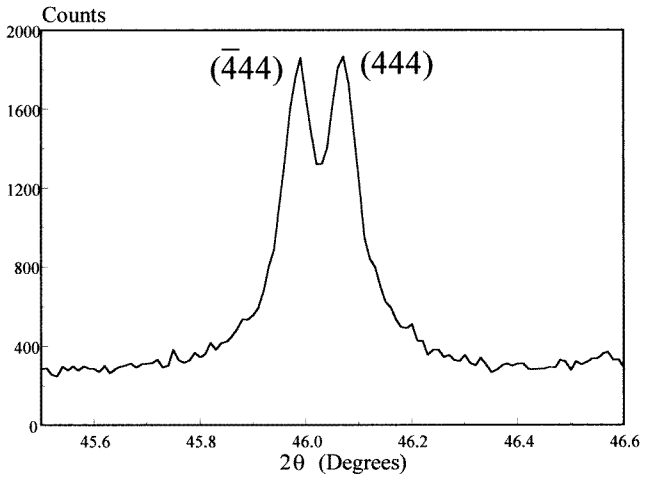

Figure 3. Splitting of the (444) reflection at 50 K in $Rb_{0.95}K_{0.05}CaF_3$, characteristic of a monoclinic symmetry.

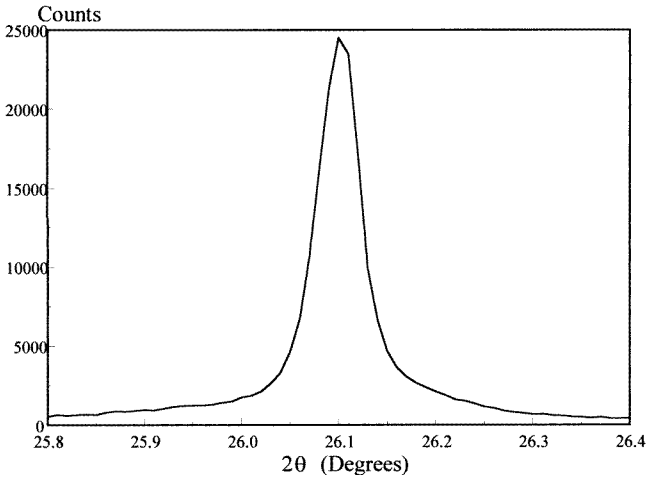

Figure 4. (400) reflections group at 50 K in $Rb_{0.95}K_{0.05}CaF_3$.

Table 2. Restrictions on ion displacements in the supercell $2a \times 2b \times 2c$ according to the tilt system $a^-a^+a^-$ and corresponding to the space group *Pnma*.

	Rb_1, K_1	Rb_2, K_2	Ca_1	Ca_2	F_1	F_2	F'_2	F_3
x	$0.25 + u_R$	$0.25 + w_R$	0	0	0.25	u_F	$-u_F$	u_F
y	0.25	0.25	0	0	$-u_F$	0.25	0.25	u_F
z	$0.25 + w_R$	$0.75 + u_R$	0	0.5	$-u_F$	$-u_F$	$0.5 + u_F$	0.25

In spite of an increase in the number of structural parameters refined (17 instead of six in SG *Pnma*), the improvement is not significant in this SG.

Therefore, the sequence of phase transitions adopted by this mixed compound is structurally the same as in pure $RbCaF_3$. A typical example of the similarity between the

Table 3. Final parameters from the Rietveld refinement of synchrotron powder diffraction data of $Rb_{0.95}K_{0.05}CaF_3$ at 50 K according to the tilt system $a^-a^+a^-$ (space group *Pnma*). *B* ($Å^2$) are isotropic Debye–Waller factors.

Cell constants:	$2a = 8.8632(2)$ Å	$\beta = 90.15(1)^\circ$
Structural parameters:		
$u_R = 0.0048(3)$	$w_R = 0.0064(3)$	$u_F = 0.0213(3)$
B(Rb, K) = 1.19(3)	B(Ca) = 0.93(3)	B(F) = 1.29(6)
Final *R*-factors:		
$R_I = 3.8\%$	$R_{wp} = 11.0\%$	$R_{exp} = 7.1\%$

structures of both compounds can be found in the octahedra tilt angle value, which takes the value $4.9(1)^\circ$ in $Rb_{0.95}K_{0.05}CaF_3$ at $T = 50$ K while a very close value of 5° at $T = 5$ K is obtained in pure $RbCaF_3$ [8]. However the mechanism of the lowest temperature phase transition is probably affected by the potassium substitution in the cell. In pure $RbCaF_3$, the violent character of this transition, evidence of a first order mechanism, was revealed by different techniques [5], whereas the displacive behaviour of this phase transition in $Rb_{0.95}K_{0.05}CaF_3$ seems to be unambiguously revealed by a Raman scattering study of this compound versus temperature [23]. This demonstrates that even a very small amount of K substitution is able to modify significantly the mechanism of the structural phase transition. This feature can be justified simply by involving the respective sizes of the K^+ and Rb^+ ions. Actually the smaller size of K^+ ions ($r_{K^+} = 1.64$ Å), compared with Rb^+ ions ($r_{Rb^+} = 1.72$ Å) makes the rotation of the CaF_6 octahedra easier, consistent with a progressive evolution of the rotation angle associated with a displacive character of the transition.

4.2. $Rb_{0.80}K_{0.20}CaF_3$

Two phase transitions also occur in this compound. From the ideal cubic symmetry, a first one was previously detected at $T_c = 255$ K, and a second at $T_c = 153$ K [14]. The sequence of phase transitions was not well established and remained confused until now [15, 24]. In particular, the intermediate symmetry between 153 and 255 K was given to be either tetragonal or orthorhombic according to different authors.

In order to study the pre-transitional effects around the higher temperature phase transition and also to determine unambiguously the sequence of phase transitions, powder diffraction scans were collected in the angular range 22–55° 2θ counting 1 s/step at 230, 200 and from 180 to 140 K in steps of 5 K. A slow scan of the low temperature phase was also recorded at 100 K from 9 to 65° 2θ (2 s/point).

4.2.1. Temperature range 295→180 K. In figure 5 is shown the evolution of the (400) reflection for some typical temperatures. At 295 K, the reflection is a single line (cubic symmetry—$a^0a^0a^0$ tilt system). In the range 230–180 K, the splitting of this reflection into two components (004) and [(400, 040)] (see figure 5 for $T = 230$ K) indicates a tetragonal symmetry ('T phase'), which is definitely confirmed by the Rietveld refinements carried out in SG $I4/mcm$ ($a^0a^0c^-$ tilt system) at 230, 200 and 180 K. The results are gathered in table 4. The tilt angle in the T phase corresponding to the rotation around the *c* axis is displayed in figure 6. One can underline that, even with a high resolution experiment, no superlattice reflection, characteristic of a lower distorted symmetry, was detected in this intermediate temperature region.

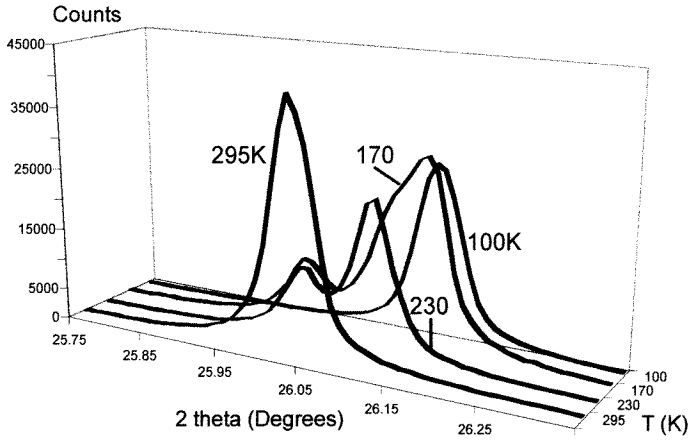

Figure 5. (400) reflections group in $Rb_{0.80}K_{0.20}CaF_3$, illustrating the symmetry changes when the temperature varies.

Table 4. Final parameters of Rietveld refinements in the tetragonal phase according to the tilt system $a^0a^0c^-$ (space group $I4/mcm$) of $Rb_{0.80}K_{0.20}CaF_3$ at 180, 200, 230 K. $\phi(^\circ)$ is the tilt angle around the c axis.

T (K)	a (Å)	c (Å)	u_F	$B_{Rb,K}$	B_{Ca}	B_F	ϕ	R_I	R_{wp}	R_{exp}
180	6.2579(1)	8.8948(1)	0.0311(5)	1.22(4)	0.73(4)	1.8(1)	7.1	3.2	10.9	8.2
200	6.2619(1)	8.8957(1)	0.0293(5)	1.60(4)	0.93(4)	2.6(1)	6.7	3	8.9	6.8
230	6.2663(1)	8.8903(1)	0.0253(6)	1.73(4)	1.06(4)	2.9(1)	5.8	2.9	9.5	7.6

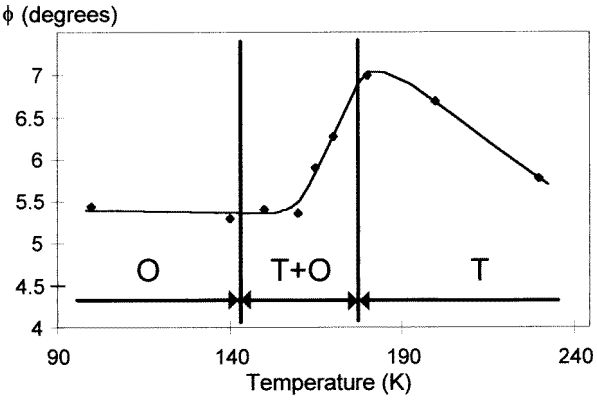

Figure 6. CaF_6 octahedron tilt angles for $Rb_{0.80}K_{0.20}CaF_3$ determined from Rietveld refinement results. O denotes the low temperature orthorhombic phase (SG $Pnma$). In the intermediate range labelled as T + O, the tilt angles have been calculated by using the values refined for the O phase, which is the major phase in the pattern for $T \leqslant 175$ K (see also figure 10).

4.2.2. Temperature range 140→100 K. In this temperature range, the powder diffraction pattern is very similar to that observed at low temperature for $Rb_{0.95}K_{0.05}CaF_3$. It exhibits the following features:

Table 5. Final parameters from the Rietveld refinement of $Rb_{0.80}K_{0.20}CaF_3$ at 100 K according to the tilt system $a^-a^+a^-$ (space group *Pnma*). An underestimated (μr) value could explain the lower temperature factors obtained for $x = 0.20$ than for $x = 0.05$.

Cell constants:	$2a = 8.8506(2)$ Å	$\beta = 90.07(1)^\circ$
Structural parameters:		
$u_R = 0.0054(6)$	$w_R = 0.0062(6)$	$u_F = 0.0281(6)$
$B(\mathrm{Rb, K}) = 0.47(3)$	$B(\mathrm{Ca}) = 0.36(2)$	$B(\mathrm{F}) = 0.74(5)$
Final *R*-factors:		
$R_I = 4.8\%$	$R_{wp} = 9.6\%$	$R_{exp} = 7.1\%$

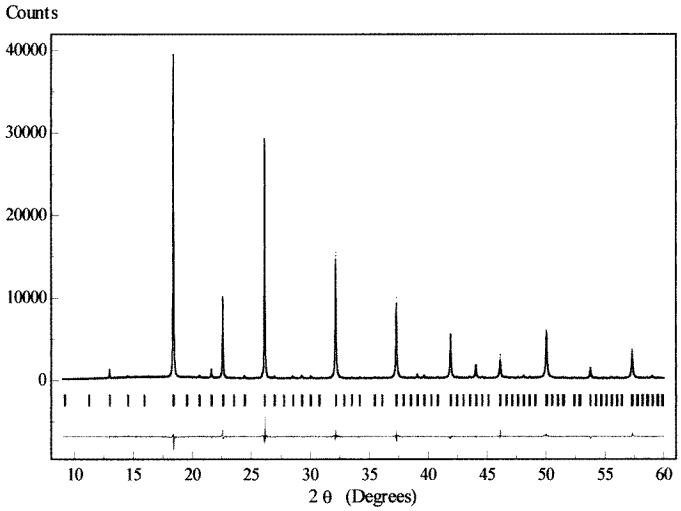

Figure 7. Observed, calculated and difference profiles for $Rb_{0.80}K_{0.20}CaF_3$ at 100 K.

(i) In addition to reflections associated with the tilt −, new superlattice reflections characteristic of a tilt + have appeared.

(ii) The splitting of the (444) reflection at $2\theta \approx 46.1^\circ$ reveals a monoclinic distortion of the supercell $2a \times 2b \times 2c$.

(iii) A quasi-single line is obtained for the (400) reflections group (figure 5) indicating very close values for the cell constants.

The Rietveld refinement at 100 K in the same SG *Pnma* as for $Rb_{0.95}K_{0.05}CaF_3$ confirms the tilt system ($a^-a^+a^-$) (orthorhombic phase or O phase). The results are given in table 5 and the profiles are illustrated in figure 7. The tilt angle (figure 6) is slightly higher ($\approx 5.4(1)^\circ$) than that obtained in $Rb_{0.95}K_{0.05}CaF_3$ at 50 K ($4.9(1)^\circ$). This result is in agreement with the previous comment about the greater ability for the CaF_6 octahedra to rotate when the K concentration increases because of its smaller size. This is correlated with the decrease of the monoclinic distortion in the supercell (figure 8). The same tilt system ($a^-a^+a^-$) was considered to refine the structure at 140 K. Moreover, once again, the refinement in the more general SG $B2_1/m$ does not yield any significant improvement.

4.2.3. Intermediate temperature range 175→140 K. Actually, the superlattice reflections characteristic of a tilt + start to appear at 175 K indicating a symmetry change with respect to

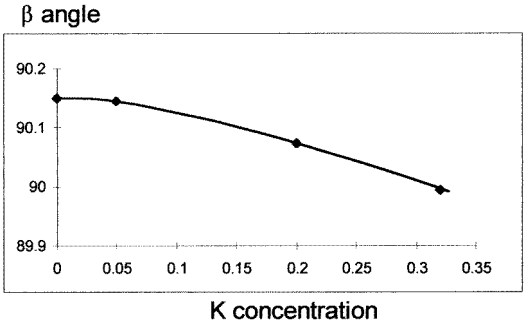

Figure 8. Evolution of the β angle characterizing the monoclinic distortion of the supercell.

the tetragonal phase. Moreover three components are clearly visible on the (400) reflections group between 175 and 160 K (figure 5 for $T = 170$ K). Below this latter temperature, the intensity of the low angle peak decreases together with a broadening. Mainly according to the former feature, a coexistence of tetragonal (T) and low temperature orthorhombic (O) phases can explain this multi-component line: both satellite lines correspond respectively to the reflections (004) and [(400, 040)] (T phase) and the central peak to the (400) reflections group (O phase), which is a quasi-single line as at 100 K because of equal values of the cell constants $2a = 2b = 2c$. For the T phase, the decrease in intensity and the simultaneous broadening of the reflections are due to a decrease of the coherently diffracting domains.

In order to confirm this phase coexistence hypothesis, Rietveld refinements using the multipattern option have been conducted for all temperatures in the intermediate range. A typical Rietveld fit is displayed in figure 9 for $T = 165$ K. The cell constants (figure 10) and scale factor values obtained from the refinements allowed us to perform a quantitative phase analysis (figure 11) which shows a rather fast decrease in the T phase proportion. The transition temperature of 153 K detected by other techniques [14] for the second transition is consistent with our results which give an O phase proportion of more than 98% at this temperature.

4.3. $Rb_{0.68}K_{0.32}CaF_3$

This concentration has not been studied until now, but a very close one ($x = 0.35$) was previously investigated by Ratuszna *et al* [15]. In $Rb_{0.65}K_{0.35}CaF_3$ two phase transitions were also reported; the first one occurs at $T = 291$ K and gives rise below this temperature to the usual tetragonal symmetry associated with the $I4/mcm$ space group ($a^0a^0c^-$ tilt system). A second transition is observed at $T = 245$ K giving rise, according to the literature, to the unusual $a^0b^+c^-$ tilt system. Consequently the structure of this low temperature phase was chosen to be fully reinvestigated in a close concentration in order to throw light on this sequence for phase transitions.

A scan in the angular range 12–58° (2 s/point) was collected at 150 K. The signal to noise ratio is unfortunately not so good as for the other samples, because of the low beam intensity when the data were collected. However the typical superlattice reflections characteristic of tilt + and − are still present. Using a pattern decomposition procedure, the (400) reflection group at $2\theta \approx 26°$ can be perfectly fitted with two components indicating that two cell constants have equal values, for instance $2a < 2b = 2c$. Moreover, as no visible splitting is observed on the (hhh) reflection, an orthorhombic lattice symmetry can

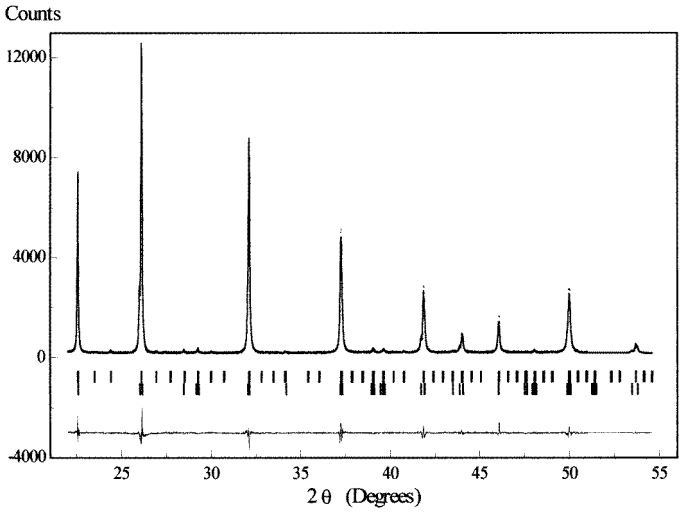

Figure 9. Part of observed, calculated and difference profiles for $Rb_{0.80}K_{0.20}CaF_3$ at 165 K. The upper and lower bars are respectively related to O and T phases.

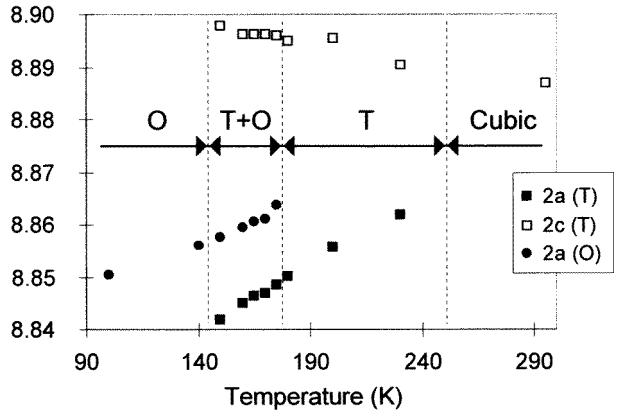

Figure 10. Cell constant values as a function of temperature in $Rb_{0.80}K_{0.20}CaF$, obtained from Rietveld refinements.

be inferred from these features, in agreement with Ratuszna *et al* [15]. According to Glazer [13], the tilt systems $a^0b^+b^-$ (SG *Bmmb*) and $a^+b^+b^-$ (SG *Pmmn*) can then be inferred, but only a Rietveld refinement is able to distinguish between these two propositions.

Actually the Rietveld refinement result is satisfactory neither in the *Bmmb* SG nor in the other *Pmmn* possibility, mainly because several lattice reflections have no calculated intensities as illustrated in figure 12. By looking at the evolution of the monoclinic β angle of the supercell $2a \times 2b \times 2c$ (figure 8) and by considering a monotonic evolution of this angle versus concentration, the predicted value for $x = 0.32$ is expected to be very close to 90°. Unfortunately, such a very weak monoclinic distortion cannot be demonstrated directly from our experimental data. Indeed a longer wavelength would be required to show evidence of a splitting on the (*hhh*) reflection.

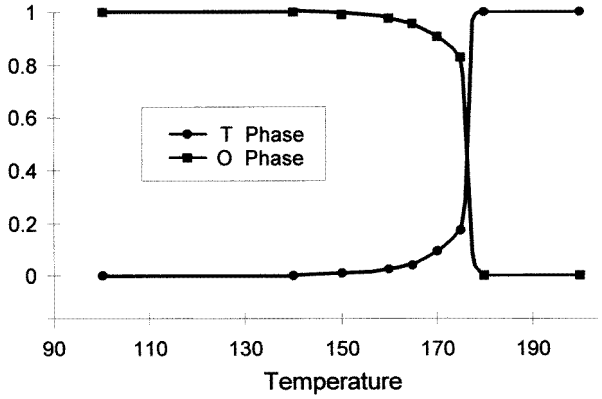

Figure 11. Quantitative phase analysis using the Rietveld method in $Rb_{0.80}K_{0.20}CaF_3$ giving the ratio of orthorhombic (O) and tetragonal (T) phases.

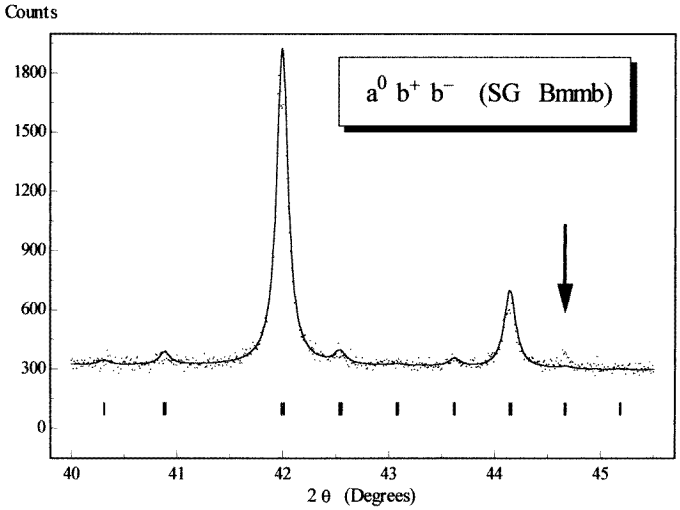

Figure 12. Part of observed and calculated profiles for $Rb_{0.68}K_{0.32}CaF_3$ at 150 K, showing that some reflections have no calculated intensities when the tilt system $a^0b^+b^-$ is considered. The same feature is observed in the tilt system $a^+b^+b^-$ (SG *Pmmn*).

Nevertheless, by making the hypothesis of such a distortion, and keeping in mind that two cell constants have equal values, a Rietveld refinement was performed in space group *Pnma* associated with the triply tilted system $a^-b^+a^-$. This yields a very satisfying calculated profile (figure 13) which justifies the tilt system $a^-b^+a^-$ at 150 K. The final structural parameters are given in table 6.

4.4. Phase diagram

The structural data obtained from high resolution powder diffraction for the $Rb_{0.95}K_{0.05}CaF_3$, $Rb_{0.8}K_{0.2}CaF_3$ and $Rb_{0.68}K_{0.32}CaF_3$ samples provide a basis to construct the phase diagram, temperature versus concentration, for this mixed system. Actually in the light of this work, it could be considered that the structures for $x < 0.5$ are fully determined.

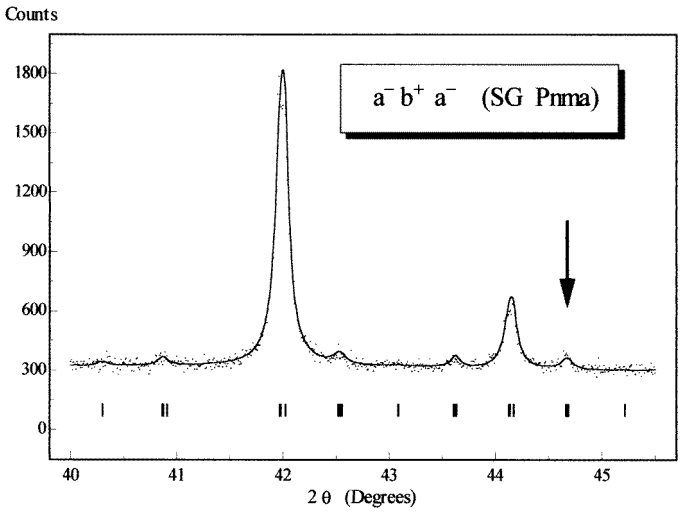

Figure 13. Part of observed and calculated profiles for $Rb_{0.68}K_{0.32}CaF_3$ at 150 K by considering the tilt system $a^-b^+a^-$.

Table 6. Final parameters from the Rietveld refinement of $Rb_{0.68}K_{0.32}CaF_3$ at 150 K according to the tilt system $a^-b^+a^-$ (space group *Pnma*). The restrictions on ion displacements in the supercell $2a \times 2b \times 2c$ are those given in table 2, except for fluorine atoms F_1 $(0.25, -u_F, v_F)$ and F_3 $(u_F, v_F, 0.25)$. However, the u_F and v_F parameters cannot be refined separately because of the rather small contribution of fluorine atoms to the diffraction peak intensities with respect to other atoms.

Cell constants:	$2a = 8.8369(2)$ Å	$\beta \cong 90^\circ$
	$2b = 8.8265(1)$ Å	
Structural parameters:		
$u_R = 0.0064(2)$	$w_R = 0.0071(2)$	$uF = 0.02667(3)$
B(Rb, K) $= 2.06(4)$	B(Ca) $= 1.74(5)$	B(F) $= 2.75(9)$
Final R-factors:		
$R_I = 7.3\%$	$R_{wp} = 13.0\%$	$R_{exp} = 11.1\%$

Beforehand table 7 summarized the transition temperatures previously measured and exhibited in the literature [5 and references therein, 9, 10, 14, 15, 25] by different techniques: ATD, DSC, birefringence, x-ray diffraction, neutron diffraction, ... Note in this table that for concentrations in the range $0.3 \leqslant x \leqslant 0.6$, three structural phase transitions are indicated. Although no clear evidence of an intermediate transition between the tetragonal phase and the orthorhombic one was previously found, it seems that weak reproducible experimental evidence from ATD, DSC, birefringence and Raman scattering experiments was observed by Daniel *et al* [25] and Hidaka *et al* [26]. Furthermore because the intermediate phase between the ideal cubic perovskite and the low temperature symmetry is either tetragonal (associated with the tilt system $a^0a^0c^-$) or orthorhombic (associated with the tilt system $a^0b^+c^-$) for mixed compounds respectively close to pure $RbCaF_3$ or to pure $KCaF_3$, it seems sensible to think that, for the compounds around $Rb_{0.5}K_{0.5}CaF_3$, the following sequence for

structural phase transitions can be suggested:

$$\begin{array}{ccccccccc} & T_{c1} & & T_{Ci} & & T_{c2} & & & \\ a^0a^0a^0 & \rightarrow & a^0a^0c^- & \rightarrow & a^0b^+c^- & \rightarrow & a^-b^+a^- \text{ or } a^-a^+a^- & \text{or } a^-b^+c^-. \\ \text{cubic} & & \text{tetragonal} & & \text{orthorhombic} & & \text{orthorhombic} & \text{or monoclinic} \\ Pm3m & & I4/mcm & & Bmmb & & Pnma & P2_1/m \end{array}$$

Table 7. Transition temperatures of mixed $Rb_{1-x}K_xCaF_3$ crystals. T_{c1} is the higher temperature transition from the ideal cubic perovskite to the tetragonal or orthorhombic symmetry. T_{c2} is the transition associated with the occurrence of the lowest temperature phase (orthorhombic or monoclinic symmetry). T_{Ci} indicates the possible location of an additional intermediate phase transition. n.m.: not yet measured.

Compound	K concentration (%)	T_{c1} (K)	T_{Ci} (K)	T_{c2} (K)
$RbCaF_3$	0	198		31.5
$Rb_{0.99}K_{0.01}CaF_3$	1	203		n.m.
$Rb_{0.95}K_{0.05}CaF_3$	5	210		74
$Rb_{0.90}K_{0.10}CaF_3$	10	250		n.m.
$Rb_{0.85}K_{0.15}CaF_3$	15	265		n.m.
$Rb_{0.80}K_{0.20}CaF_3$	20	255		153
$Rb_{0.70}K_{0.30}CaF_3$	30	295	278	n.m.
$Rb_{0.68}K_{0.32}CaF_3$	32	300	276	245
$Rb_{0.65}K_{0.35}CaF_3$	35	291	280	245
$Rb_{0.60}K_{0.40}CaF_3$	40	324	319	n.m.
$Rb_{0.53}K_{0.47}CaF_3$	47	325	310	280
$Rb_{0.50}K_{0.50}CaF_3$	50	363	361	338
$Rb_{0.30}K_{0.70}CaF_3$	70	431		409
$Rb_{0.12}K_{0.88}CaF_3$	88	516		500
$KCaF_3$	100	557		548

Note however that because of the high statistical disorder existing near $x = 0.5$, this intermediate transition labelled as T_{Ci} is necessarily 'soft' and progressive, hence justifying the weakness of experimental evidence showing its existence.

In order to throw light on the behaviour of the phase diagram adopted by these mixed $Rb_{1-x}K_xCaF_3$ disordered crystals, the model of Bhattacharya and Chakrabarti [27] was applied. This model, which predicts the evolution of transition temperatures versus impurity concentration for displacive systems with strong crystal defects, is based on the following classical Hamiltonian [28]:

$$\mathcal{H} = \sum_i \frac{m}{2}\left(\frac{\mathrm{d}\psi_i}{\mathrm{d}t}\right)^2 + \sum_i (\tfrac{1}{2}A_i\psi_i^2 + \tfrac{1}{4}B_i\psi_i^4) - h\sum_i \psi_i - \sum_{i,j} \tfrac{1}{2}J_{ij}\psi_i\psi_j \qquad (1)$$

where ψ_i correspond to the soft mode coordinates responsible for the phase transition for each unit cell i. The first term $\sum_i (m/2)(\mathrm{d}\psi_i/\mathrm{d}t)^2$ is the kinetic energy with m the effective mass of the cell. The second one $\sum_i (\frac{1}{2}A_i\psi_i^2 + \frac{1}{4}B_i\psi_i^4)$ is a classical Taylor expansion of the potential energy where $\sum_i \frac{1}{2}A_i\psi_i^2$ is associated with the harmonic component. The third term $(-h\sum_i \psi_i)$ corresponds to an external field and the last one $(-\sum_{i,j} \frac{1}{2}J_{ij}\psi_i\psi_j)$ takes into account the coupling interaction between two unit cells (defective or normal). The parameter A_i associated with the second derivative of the potential represents an average inter-atomic force constant, weighted by atomic masses, for one cell. This A_i parameter can take two values

$$A_i = A + \Delta A\, c_i$$

where $c_i = 1$ if the ith site is occupied by an impurity atom with the parameter value $A + \Delta A$ and $c_i = 0$ otherwise. Consequently it can be roughly considered that A_i is the force constant involved in the substitutional disorder which corresponds in the $Rb_{1-x}K_xCaF_3$ samples studied here, to the Rb–F ($A_i = A$) or K–F ($A_i = A + \Delta A$) interactions. From the expression (1) and by using the method of the replica trick [29] in the mean field approximation, the Hamiltonian of the system can be decomposed in two components as follows:

$$\mathcal{H} = \mathcal{H}_0 + \mathcal{H}_1$$

where $\mathcal{H}_1$ represents the additional perturbing Hamiltonian due to impurities over the configurational average Hamiltonian $\mathcal{H}_0$. Then considering a first order perturbation expansion, the free energy of this system can be expressed as

$$F = F_0 + F_1$$

with:

$$F_0 = \tfrac{1}{2}(A + 3B\sigma)\psi_0^2 + \tfrac{1}{4}B\psi_0^4 - \tfrac{1}{2}J_0\psi_0^2 - h\psi_0 + \tfrac{1}{2}A\sigma + \tfrac{3}{4}B\sigma^2 - \frac{1}{2\beta}\ln\sigma \tag{2}$$

and:

$$F_1 = -\frac{1}{\beta}\ln(1 - x + x\,\mathrm{e}^{-\frac{1}{2}\beta\Delta A(\psi_0^2+\sigma)}) \tag{3}$$

where ψ_0 denotes the equilibrium position defined by $\psi_i = \psi_0 + \Delta\psi_i$, $\sigma = \langle\Delta\psi_i^2\rangle$ and $J_0 = \sum_i J_{ij}$. x is the concentration of impurities in the system, that are here the proportion of K ions in $RbCaF_3$. $\beta = 1/kT$ where k is the Boltzmann constant. By minimizing the free energy with respect to ψ_0 and σ, one obtains the expression for the transition temperature

$$T_c(x) = T_c(x = 0)\left[1 - \frac{x\,\Delta A}{(J_0 - A)(x + (1 - x)\,\mathrm{e}^{\Delta A/2J_0})}\right] \tag{4}$$

where $T_c(x = 0)$ is then the transition(s) temperature(s) occurring in pure $RbCaF_3$ ($T_{c1} = 198$ K and $T_{c2} = 31.5$ K).

By fitting this expression to the experimental transition temperatures (given in table 7), a theoretical evolution for T_c versus the concentration x can be suggested as illustrated in figure 14. Note on this diagram that the intermediate transition is figured by a long dashed line not fitted with this former model because of the unclear evidence of its existence; moreover the vertical dotted lines correspond on this figure to the rough location where the changes of tilt system $a^-a^+a^- \rightarrow a^-b^+a^-$ and $a^-b^+a^- \rightarrow a^-b^+c^-$ occur. The structural modification associated with this evolution is obviously progressive and, actually, corresponds only to a weak evolution versus concentration of the tilt angles of CaF_6 octahedra.

Table 8. Set of parameters obtained from the model of Bhattacharya and Chakrabarti ([27]).

Transition	A (USI)	ΔA (USI)	J_0 (USI)
T_{c1}: cubic → tetragonal or orthorhombic $a^0a^0a^0$ $a^0a^0c^-$ or $a^0b^+c^-$	5.54	1.82	4.58
T_{c2}: tetragonal or orthorhombic → orthorhombic or monoclinic $a^0a^0c^-$ or $a^0b^+c^-$ $a^-b^+a^-$ or $a^-a^+a^-$ or $a^-b^+c^-$	−4.59	3.65	−4.82

The best set of parameters deduced from the model of Bhattacharya and Chakrabarti [27] is given in table 8. Special attention was paid to the parameter $\Delta A/A$ which corresponds

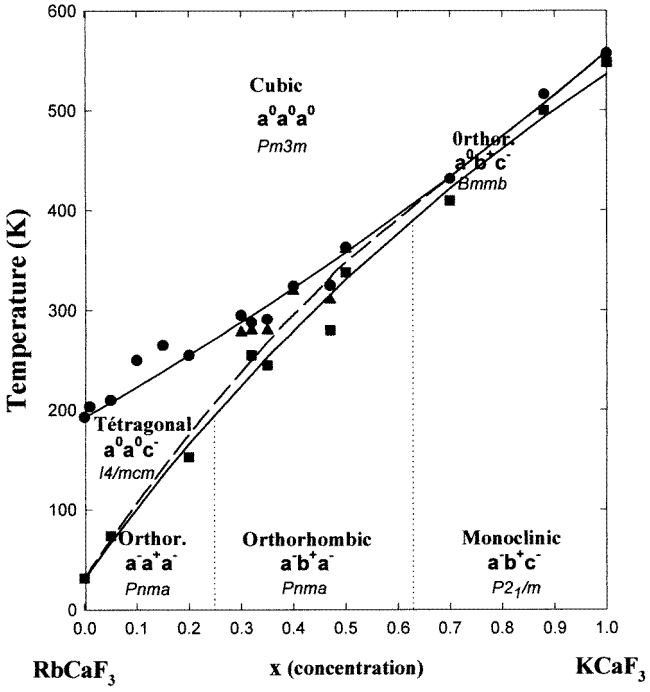

Figure 14. Phase diagram of transition temperature versus concentration, for mixed perovskite crystals $Rb_{1-x}K_xCaF_3$. Solid lines correspond to the best fit obtained with the model of Bhattacharya and Chakrabarti ([27]). Solid circles indicate experimental temperature transitions T_{c1} between the ideal cubic symmetry and a tetragonal or orthorhombic one. Solid squares correspond to the experimental low temperature transitions T_{c2}. Solid triangles are associated with evidence for an additional intermediate transition named T_{Ci}. The long dashed line is a guide for the eye concerning this former transition. Dotted lines indicate approximate location of change of tilt system versus concentration.

to the relative variation of the average inter-atomic force constant, due to the substitution by K ion impurities in the host crystal $RbCaF_3$. As previously discussed, this force constant introduced in the Hamiltonian given by equation (1) is actually defined as an average on the whole cubic unit cell and then, can be very roughly associated with the fluorine–monovalent ion (Rb or K) interaction. The $\Delta A/A$ theoretical value, deduced from the best fit obtained with the applied model, has to be compared with the experimental one defined by:

$$\frac{\Delta A}{A} = \frac{A_{K-F} - A_{Rb-F}}{A_{Rb-F}}. \tag{5}$$

The experimental force constants, given in (5), have been previously obtained by refining a lattice dynamics model on inelastic neutron scattering experimental data and they are summarized in the review paper for fluoroperovskites of Salaün and Rousseau [30].

Then we obtain

$$\left.\frac{\Delta A}{A}\right]_{theoretical} \approx 32\% \qquad \left.\frac{\Delta A}{A}\right]_{experimental} \approx 40\% \tag{6}$$

The rather good agreement obtained for these calculations seems to confirm the validity of the applied model despite its roughness.

Furthermore the sign attributed to the *A* parameter gives an indication of the character of the phase transition: the positive value obtained in the case of the high temperature phase transition is evidence of the displacive character of this transition, while the negative value obtained for the lower temperature phase transition indicates the probable order–disorder character of this second transition.

5. Conclusion

In this paper, the crystal structures of three typical mixed perovskites from the $Rb_{1-x}K_xCaF_3$ system were investigated by high resolution powder diffraction. The ambiguities about the phase transition sequences occurring in these compounds now seem to be fully removed. Furthermore, in the light of these results as well as others obtained in these compounds from previous studies using other techniques, a phase diagram has been proposed and refined according to the phenomenological model of Bhattacharya and Chakrabarti [27].

On the basis of this work, Raman spectra and vibrational investigation by neutron scattering could be more easily interpreted. Especially with this reliable structural study, investigation of transitional mechanisms in the general perovskite family formed by rigid octahedra entities, showing high anisotropy between octahedra layers, could be approached with better accuracy. This aspect is in progress.

Acknowledgments

We thank the CCLRC Daresbury Laboratory for the provision of beam time on station 9.1 under the European Large Facilities Programme, contract number 28132. We are grateful to Professors M Rousseau, J Y Buzaré and A Bulou for fruitful discussions and suggestions around this paper. Also we wish to thank Professor J Nouet and G Niesseron for invaluable help in the growth of crystal samples as well as Dr G Silly for assistance in the synchrotron radiation experiments.

References

[1] Cowley R A 1980 *Adv. Phys.* **29** 1 and references therein
[2] Bruce A D 1980 *Adv. Phys.* **29** 111 and references therein
[3] Bruce A D and Cowley R A 1980 *Adv. Phys.* **29** 219 and references therein
[4] Modine F A, Sonder E, Unruh W P, Finch C B and Westbrook R D 1974 *Phys. Rev.* B **10** 1623
[5] Daniel Ph, Rousseau M and Toulouse J 1997 *Phys. Rev.* B **55** 6222
[6] Fleury P A, Scott J F and Worlock J M 1968 *Phys. Rev. Lett.* **21** 16
[7] Martin J J, Dixon G S and Velasco P P 1976 *Phys. Rev.* B **14** 2609
[8] Bulou A, Ridou C, Rousseau M, Nouet J and Hewat A W 1980 *J. Physique* **41** 87
[9] Bulou A, Nouet J, Hewat A W and Schäfer F J 1980 *Ferroelectrics* **25** 375
[10] Hidaka M, Yamashita S and Okamoto Y 1984 *Phys. Status Solidi* a **81** 177
[11] Rousseau M, Daniel Ph and Hennion B 1997 *J. Phys.: Condens. Matter* **9** 8963
[12] Ratuszna A, Rousseau M and Daniel Ph 1997 *Powder Diffraction* **12** 70
[13] Glazer A M 1975 *Acta Crystallogr.* A **31** 756
[14] Foucher P, Buzaré J Y, Ridou C, Rousseau M and Hennion B 1990 *Ferroelectrics* **107** 325
[15] Ratuszna A, Daniel Ph and Rousseau M 1995 *Phase Transitions* **54** 43
[16] Nouet J 1997 *Proc. SPIE* 3178
[17] Rietveld H M 1969 *J. Appl. Crystallogr.* **2** 65
[18] Murray A D and Fitch A N 1989 *MPROF, a Multipattern Rietveld Refinement Program for Neutron, X-ray and Synchrotron Radiation* (London: University College)
[19] Ibers J A and Hamilton W C (eds) 1974 *International Tables for X-ray Crystallography* vol 4 (Birmingham: Kynoch)

[20] Sasaki S 1989 *KEK Report* 88-14
[21] LeBail A and Jouanneaux A 1997 *J. Appl. Crystallogr.* **30** 265
[22] Caglioti G, Paoletti A and Ricci F P 1958 *Nucl. Instrum.* **3** 223
[23] Daniel Ph, Toulouse J and Rousseau M 1998 *Phys. Rev.* B submitted
[24] Debaud-Minorel A M 1993 *PHD Thesis* Université de Caen (Le Mans: Université du Maine)
[25] Daniel Ph, Toulouse J, Rousseau M, Désert A and Ratuszna A 1998 *Phil. Mag.* submitted
[26] Hidaka M, Zhou Z Y and Yamashita S 1990 *Phase Transitions* **20** 83
[27] Bhattacharya S and Chakrabarti B K 1983 *Solid State Commun.* **45** 293
[28] Halperin B I and Varma C M 1976 *Phys. Rev.* B **14** 4030
[29] Chakrabarti B K 1981 *Z. Phys.* B **43** 1
[30] Salaün S and Rousseau M 1997 *Phys. Rev.* B **51** 15 867